Identification of Induction Machine Rotor Parameters at any Operating Point Considering Temperature dependent Permeability

W. Fahrner
Department of Energy Systems and Electrical Drives
Vienna University of Technology
Vienna, Austria
walter.fahrner@tuwien.ac.at

M.A. Vogelsberger
Product and R&D_Management
RoQ_M_DRIVES
Bombardier Transportation Austria GmbH
Vienna, Austria
markus.vogelsberger@rail.bombardier.com

T. Wolbank
Department of Energy Systems and Electrical Drives
Vienna University of Technology
Vienna, Austria
thomas.wolbank@tuwien.ac.at

***Abstract*— The investigation presented in this paper aimed to analyze the temperature dependences of induction machine parameters. More specifically, the focus was placed on the temperature behavior of magnetic properties. The machine under test is a 100kW traction motor used in standard railway applications. Knowledge of parameters temperature dependences is necessary to ensure precise operation of the induction machine over a wide temperature range. Therefore, measurements for different stator and rotor temperatures of the machine were conducted, which revealed that the permeability of the stator and rotor side electrical steel sheet show a clear temperature dependence. Moreover, a reduction of flux density due to increasing temperature was determined. The purpose of these results is to improve the accuracy of stator or rotor equation-based flux models.**

Keywords— induction machine, rotor parameters, permeability, temperature dependence

I. INTRODUCTION

Induction machines (IMs) are widely used in traction drive applications like railway systems and the automotive industry. Much progress has been made in development of accurate torque control structures for induction machine drives. The main problem of electrical drives used in this field is the requirement of precise operation within a wide temperature range.

The most commonly-known torque control methods for IMs are direct torque control (DTC) and field orientated control (FOC). The performance of both methods depends on an accurate calculation of flux linkage, which is accomplished by using flux models based on rotor and/or stator equations of the IM. Consequently, one key point is the accurate determination of all machine parameters. In addition, knowledge of the temperature dependences of all parameters is necessary to guarantee high performance over a wide temperature range. Especially with the rotor side parameters, the identification and adaptation of temperature dependence can be challenging when the drive operates at a low speed for long time periods. Therefore, significant research has focused on rotor temperature and rotor resistance identification techniques [1]-[3], whereas research has rarely been conducted concerning the temperature dependence of magnetic properties, like the permeability and flux density of IMs. One promising approach for on-line rotor parameter detection is based on analysis of inherent machine saliencies. More particularly, the properties of the spatial saturation saliency are used to estimate the rotor time constant. A detailed description of this approach can be found in [4] and [5]. For this approach, the assumption was made that the inductance remains constant over temperature. Knowledge of temperature dependence of the IM's inductance can thus be used to improve accuracy of the estimation. Inductance change is caused by permeability variation of the material over temperature, whereby this effect is discussed in some publications. Investigations of magnetic properties behavior over temperature for different material probes can be found in [6] and [7]. There are some differences in the change of permeability with increased temperature. The permeability at low flux density is increased with temperature (Hopkinson effect [8]) and that at higher flux density it is reduced with temperature. A further temperature effect is the variation in flux density with temperature [9], which adversely influences the machine torque capability.

The investigation presented in this paper is based on saliency extraction methods that were initially developed for usage in speed sensorless control. The ability to identify and extract machine saliencies is linked with an excitation of the machine with high frequencies. Accordingly, the influence of symmetrical fundamental wave properties weakens, and the influence of asymmetries like slotting and spatial saturation becomes dominant.

Usually, saliency extraction is accomplished by measuring the current response caused by additional voltage excitation, distinct in frequency from the fundamental wave. The method of excitation can be classified into high frequency carrier signals and voltage pulses [10]-[17]. A carrier signal (typically in the range of several hundred Hz) is superimposed to the fundamental wave excitation. The saliency extraction method used in this study is based on voltage pulse injection. These pulse excitations can be either established separated from PWM or integrated into the fundamental wave PWM excitation. The resulting current responses due to voltage excitation are derived in time. The following analysis of calculated derivatives provides information about magnetic properties of the electrical steel sheet. More precisely, the average current derivative reflects the value of fundamental wave inductance. Furthermore, the level of spatial stator saturation is determined by the modulation amount of current derivative. In general, there are two dominant modulation effects that arise in IMs, caused by saturation and rotor slotting. Additionally, an intermodulation also appears as a combination of these two spatial modulations.

978-1-7281-4878-6/19/$31.00 ©2019 IEEE

In order to identify temperature dependences, measurements were conducted at different stator and rotor temperatures. In view of the differences in temperature behavior of permeability, measurements were also performed without magnetization and for different magnetization levels of the IM.

The remainder of this paper is organized as follows. The method used for the extraction of magnetic properties is presented in section II, while an overview of thermo magnetic effects can be found in section III. Section IV includes measurement results without magnetization of the machine and different stator and rotor temperatures. In addition, measurement results for various levels of magnetization and temperatures are presented. Moreover, a detailed discussion of the results is provided within this section.

II. METHODOLOGY

All measurements presented in this study were generated using voltage pulse excitation of the IM. The excitation and evaluation techniques were realized in LabView and implemented on a laboratory test rig. In addition, the machine control and data acquisition were also performed in LabView. The control method is based on standard FOC. Voltage pulse excitation was realized within one PWM period. Therefore, every tenth PWM period was used to apply the voltage pulse pattern instead of the standard PWM sequence. According to the classical INFORM calculation [18], the injection of six different voltage pulses is required to compound one current-derivative-phasor. Consequently, one PWM period was sequentially used to inject the voltage pulse pattern (+U/-U, +V/-V or +W/-W respectively). All measurements in this paper were taken by this cyclic pulse excitation. Current responses due to the injected voltage pulse pattern were stored for further analysis, aiming to detect changes in the magnetic properties of the rotor and stator side electrical steel sheet.

The following description is separated into sections regarding the extraction of magnetic properties and test rig.

A. Extraction of Magnetic Properties

The purpose of the following section is to provide a brief overview of saliency extraction based on INFORM method. For a detailed description, reference is made to [18].

Transient machine current reaction as a result of pulse excitation is determined by the stator equation.

$$\underline{v_s} = r_s \cdot \underline{i_s} + \underline{l_{l,t}} \cdot \frac{d\underline{i_s}}{d\tau} + \frac{d\underline{\lambda_R}}{d\tau} \tag{1}$$

In this equation, $\underline{v_s}$ depicts the injected voltage phasor, which initiates the resulting stator current reaction $\underline{i_s}$. The rotor flux linkage is given by $\underline{\lambda_R}$. In this equation, quantity $\underline{l_{l,t}}$ differs from the fundamental wave leakage inductance. It additionally carries information about inherent machine saliencies. Therefore, $\underline{l_{l,t}}$ can be separated into a constant and a modulated part (2).

$$\underline{l_{l,t}} = l_{average} + \sum l_{mod} \cdot e^{i \cdot \varphi} \tag{2}$$

The quantity $l_{average}$ in equation (2) represents symmetrical machine parameters (constant part resulting from fundamental wave), while the second term describes all spatial modulations caused by different saliency effects of the machine. In view of the fact that only the quantity $\underline{l_{l,t}}$ contains inductance information, the influence of the stator resistance and back EMF need to be eliminated from equation (1), which is accomplished by subtracting two measurement results from the antiparallel voltage phasors (e.g. +U/-U). The next step is to calculate the time derivative of all current responses due to each active voltage phasor. An inverter comprising three half bridges is capable of applying six active voltage phasors to the machine. In this manner, a current-derivative-phasor can be composed. Therefore, every injected active voltage phasor corresponds to one component of the current-derivative-phasor, pointing dominantly in injection direction. If this method is used for speed sensorless control, a further step is needed to remove the offset from equation (2). This can be achieved by combination of the results obtained from the injection of the three phase directions (U,V,W) to one phasor. Consequently, the resulting phasor only contains asymmetry information related to machines saliencies as well as their modulations. This saliency information can further be used e.g. for rotor position tracking.

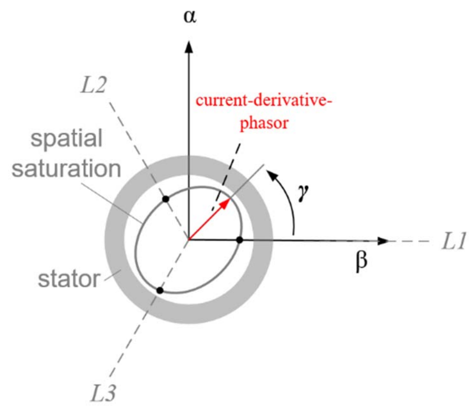

Fig. 1. Schematic depiction of spatial saturation.

A simplified example of the current-derivative-phasor comprising only one single saliency effect (caused by spatial saturation) appears as given in Fig. 1. The spatial saturation level is depicted in this figure as an elliptic trace in the stator fixed reference frame of the machine with its main axis pointing in the direction of maximum saturation. Therefore, the phase values of the saturation level can be represented as black dots on the intersection of the ellipse and the corresponding phase axes (for simplicity, dots are only depicted on positive phase axes). The saturation level can be approximated proportional to the magnitude of the resulting phase current time derivative. Accordingly, the resulting current-derivative-phasor (red arrow) is obtained. Its angular orientation is defined by the main axis of the ellipse and its magnitude by the ratio of axes of the ellipse.

Given that the investigations conducted in this study are related to the temperature dependence of magnetic properties, symmetrical (fundamental wave) and asymmetrical effects (saliency effects) are analyzed. Accordingly, the removal of the offset was omitted. Hence, all analyzed current-derivative-phasors in this paper contain the offset and the modulated part of equation (2).

B. Experimental Test Rig

The entire measurement and control system is depicted in the block diagram 0 schematically. The test rig comprises a load machine and the machine under test (denoted ‘Induction machine’ in the figure). Each machine is fed by a standard industrial IGBT-inverter. For FOC in combination with a current model (based on rotor equation), a rotor position sensor (shaft encoder) is mounted on the rotor shaft. Rotor temperature can be measured using an infrared measuring device, which is placed in a hole, drilled in the bearing housing close to the rotor ring. In addition, there are temperature sensors integrated in the stator iron. Moreover, there is one sensor for current measurement in each phase. The machine control is implemented on a real-time control system as mentioned above. A traction motor for standard railway applications is used as machine under test. The stator of the IM features a water cooling system, connected to a temperature control unit. Thus, it is possible to keep the stator temperature constant to different levels. Due to the long thermal time constants of rotor iron and copper, warming up of the rotor is accomplished by running the machine with rated torque for several hours.

For this investigation, voltage pulse injections for extraction of magnetic properties are applied separated from the fundamental wave PWM excitation. Therefore, periodically a single PWM cycle is selected for voltage pulse injection. The PWM frequency is set to 2,5kHz, resulting in a duration of 400µs for a single excitation cycle. During the cycle, a pulse sequence with zero average voltage is applied and the current controller is modified accordingly.

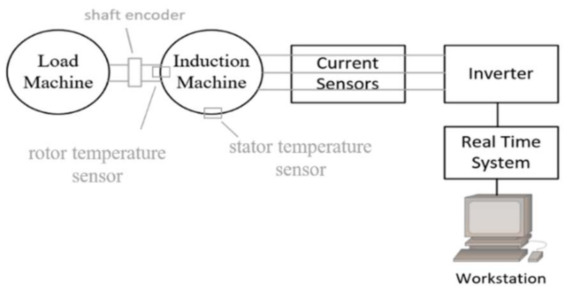

Fig. 2. Schematic illustration of the experimental test rig.

III. TEMPERATURE EFFECTS ON MAGNETIC PROPERTIES

Within this section, a brief overview of temperature effects on magnetic properties will be given. A more detailed description can be found in [8] and [9]. The focus should be on temperature dependence of initial permeability and magnetization of ferromagnetic materials.

As already mentioned in the introduction, there are some differences in the change of permeability with increased temperature. The permeability of unmagnetized materials (in literature denoted as initial permeability) is increased with temperature. This behavior is also known as Hopkinson effect. However, permeability of magnetized materials is reduced with increasing temperature. Both effects are discussed following:

A. Temperature Dependence of Initial Permeability

It is commonly known that the initial permeability reduces drastically close to the Curie temperature (CT) and reaches the value one above this temperature. Furthermore, initial permeability increases with temperature below the CT. Fig. 3Fig. 3Fig. 3 shows a typical characteristic of the initial permeability over temperature for ferromagnetic materials.

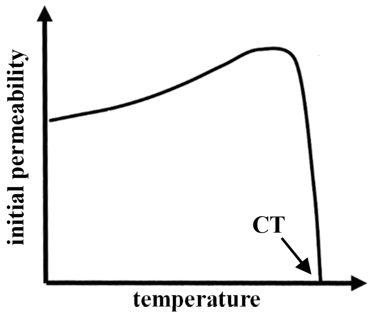

Fig. 3. Schematic diagram of initial permeability over temperature [19].

B. Temperature Dependence of Magnetization

Together with magnetic flux level, temperature is one main factor in causing change in magnetization. Fig. 4 depicts the characteristic of the intrinsic induction over temperature for different field strengths H. An iron specimen which is exposed to a high magnetic field, shows a continuously decrease in induction/permeability with increasing temperature. Moreover, the induction declines rapidly at the CT. When the field strength is lowered, the curve is becoming increasingly similar to the characteristic of the initial permeability. The intrinsic induction will first increase with rising temperature. After passing through a maximum, the intrinsic induction will decline rapidly again [9].

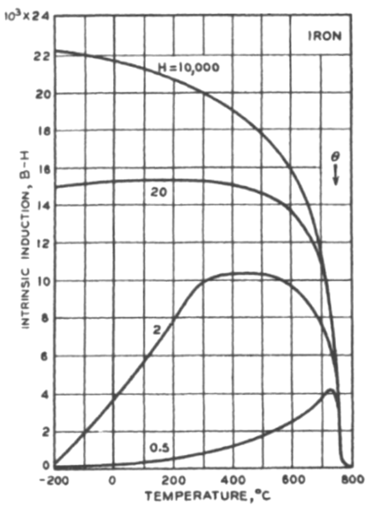

Fig. 4. Characteristic of intrinsic induction for different field strengths H. The figure is taken from [9].

IV. RESULTS AND DISCUSSION

Within this chapter, a detailed presentation of all conducted measurements will be provided. Furthermore, a discussion of the correlations between temperature and permeability found in the analysis will be included. The chapter is divided into sections regarding results without magnetization and with different levels of magnetization. The purpose of measurements without magnetization is, to find correlations between temperature and initial permeability. However, measurements with magnetization were conducted to investigate, how temperature behavior of permeability is influenced by the level of magnetization.

A. Measurement Initial Permeability Dependence on Temperature

This section aims to investigate the temperature dependence of initial permeability. Therefore, voltage pulses were injected into the machine without a magnetization of the machine. In addition, the speed of the machine under test was kept constant by the load machine to 10rpm. Measurements were conducted for different stator and rotor temperatures.

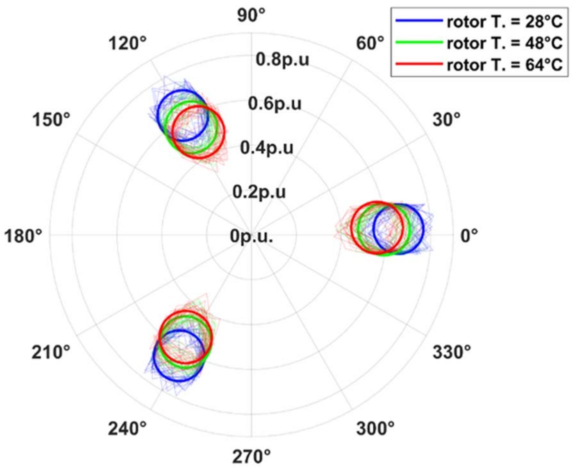

Fig. 5. Traces of the three current-derivative-phasor components for unmagnetized machine. Stator temperature kept constant at 22°C. To improve clarity, constant part is reduced by factor 20.

Fig. 5 shows the traces of the three current-derivative-phasor components obtained for excitation in the three main phase directions during one mechanical revolution of the rotor. As the machine is operated with zero flux level, the only modulation effect visible is due to rotor slotting. In order to make the temperature influence clearly visible, a least-squares circle fit function was used. Stator temperature was kept constant at 22°C and the rotor temperature was changed to three different values. The radius of the circles correlates with quantity of modulation due to rotor slotting. However, the positions of circle centers are related to the reciprocal value of the average inductance. This value matches the quantity, denoted $l_{average}$ in equation (2). It can clearly be seen that the circle centers move towards the origin of the diagram with increasing rotor temperature. This behavior corresponds to increasing inductance values with rising rotor temperature. While the quantity of rotor slotting modulations (radius of circles) remains unaffected by rotor temperature as this effect is dominantly caused by geometrical properties. All of this suggests that the permeability of the rotor side electrical steel sheet increases with temperature.

It has to be stressed, that the ratio between the constant part and the modulated part of inductance is about 100:1. Hence, in order to better illustrate these considerations, the constant part was rescaled by a factor of 20 in Fig. 5.

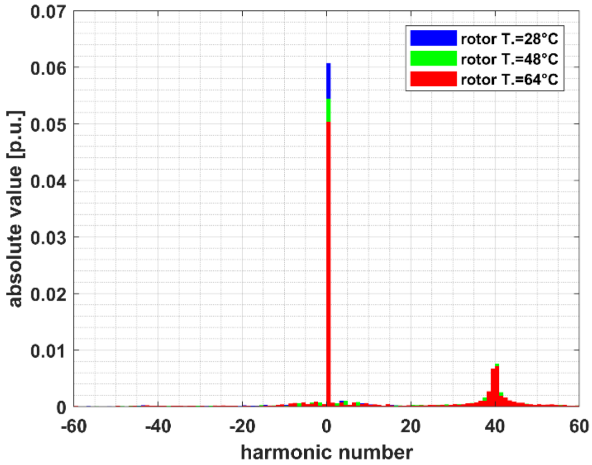

Fig. 6. Spectra of one current-derivative-phasor component depicted in Fig. 5. Measurements conducted with constant stator temperature 22°C and different rotor temperature (28° blue, 48° green, 64° red, unmagnetized machine. To improve clarity, constant part (offset) is rescaled by a factor of 20.

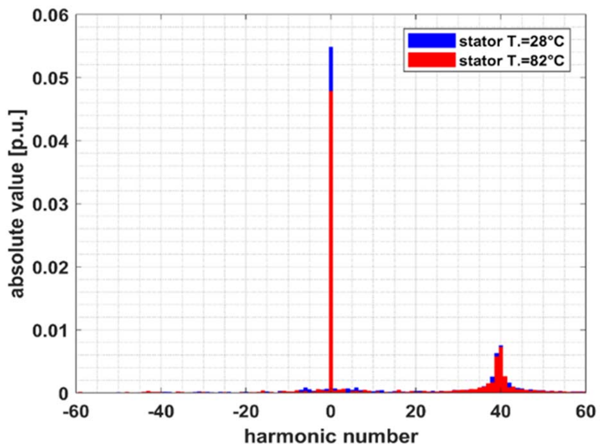

Fig. 7. Spectra of one current-derivative-phasor component for constant rotor temperature of 45°C and varied stator temperature. (28° blue, 82° red); unmagnetized machine. To improve clarity, constant part (offset) is rescaled by a factor of 20.

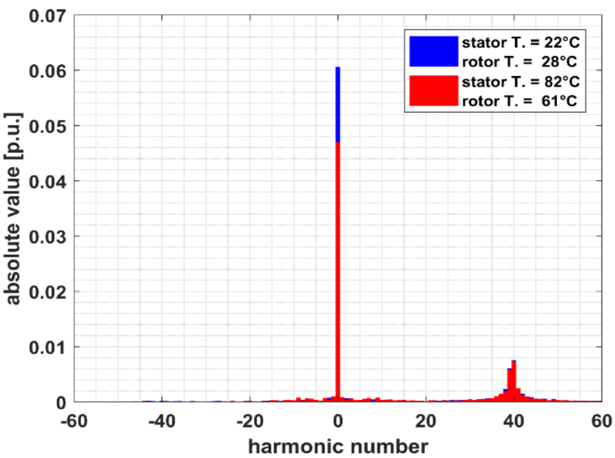

Fig. 8. Spectra of one current-derivative-phasor component for stator and rotor at room temperature (stator 22°/rotor 28° blue), and warmed-up machine (stator 82°/rotor 61° red) unmagnetized machine. To improve clarity, constant part (offset) is rescaled by a factor of 20.

For the purpose of deeper investigation, a spectral analysis was used. The spectra of one component of the current-derivative-phasor (from the direction of excitation +U/-U) from Fig. 5 is depicted in Fig. 6. The rotor slotting number of the machine under test is 40. Consequently, the modulation due to rotor slotting becomes the harmonic number of 40 within the spectra. Furthermore, the reciprocal value of the average inductance $l_{average}$ is represented by the harmonic number zero. The graph can thus be used to calculate the rate of permeability change. The change of permeability due to a rotor temperature increase of 20°C amounts to 6.31‰, while a rotor temperature increase of 36°C results in a permeability increase of 9.4‰. Hence, the average rate of permeability change at the rotor side within the considered temperature range is calculated to 0.26‰/°C.

Similar behavior was found if the stator was changed while keeping rotor temperature constant. Again, increasing temperature leads to rising permeability at the stator side electrical steel sheet. The measurement results depicted in Fig. 7 were achieved by a constant rotor temperature of 45°C and different stator temperatures. The change of permeability due to a stator temperature increase of 54°C amounts to 6.2‰. This results in an average rate of change for the stator side of 0.12‰/°C within the considered temperature range.

A comparison of the warmed-up machine with the machine under room temperature is presented in Fig. 8, whereby the resulting change of permeability due to warming up the whole machine (stator Δ ~ +60°; rotor Δ ~ +30°) amounts to 13.3‰. This value is significant higher compared to the other two measurements. The reason for this is, that in this case the permeability of the stator side as well as the rotor side electrical steel sheet is increased.

B. Change of Permeability with Magnetization Current and Temperature

The following section aims to study the temperature influence on permeability for different magnetization levels of the machine. Therefore, magnetization current was increased from zero in 10% steps. The magnetizing current is expressed as percentage of the rated current. Again, the speed of the machine under test was held constant at 10rpm by the load machine. Furthermore, all measurements were again conducted with unloaded rotor.

Fig. 9 shows the characteristic of average inductance over magnetization current for different rotor temperatures and a constant stator temperature of 22°C. The rotor temperature difference amounts to 36°C. As can be clearly seen, at the lower range of magnetization current, behavior of permeability is determined by the Hopkinson effect. In accordance with the results presented in section IV.A, the average inductance increases with temperature. Again, this suggests that increasing temperature leads to rising permeability of the rotor side electrical steel sheet. This dependence is weakened for higher levels of magnetization and finally undergoes a reverse when the electrical steel sheet is saturated. The two curves depicted in the diagram intersect at a magnetization current of approx. 47%. At this specific point, permeability is decreased with the increase of rotor temperature. This means that the flux density of the machine becomes reduced with increased temperature.

In order to verify this behavior, additional measurements were conducted with a rotor temperature difference of 16°C and a constant stator temperature of 25°C. These results are presented in Fig. 10. The obtained correlations between the magnetization current and the average inductance are similar to the previous results. The intersection of these two curves is at approx. 40% of the rated current. Due to the lower rotor temperature difference the influence of the Hopkinson effect is reduced compared to the results depicted in Fig. 9.

In addition, measurements by warmed-up machine and the machine at room temperature were conducted. The stator temperature of the warmed up machine is 82°C, whereby temperature of the rotor amounts to 61°C. By contrast to previous results, both, stator and rotor temperature was significant varied. This means that permeability of the stator side as well as the rotor side electrical steel sheet is increased by temperature. Consequently, the characteristics depicted in Fig. 11 exhibits a high deviation of their average inductances. This deviation becomes smaller with increasing level of

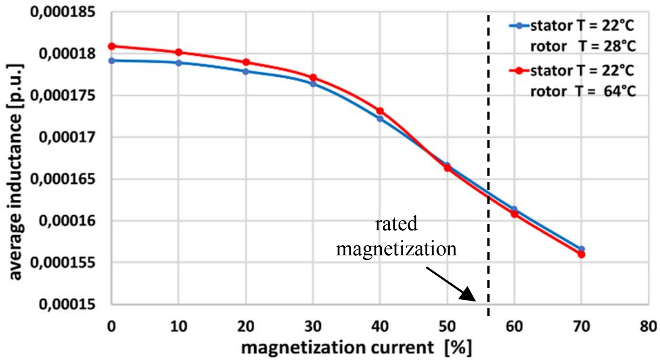

Fig. 9. Characteristic of average inductance over magnetizing current for different rotor temperatures (28° blue, 64°red) and constant stator temperature of 22°C. Magnetizing current is expressed as percentage of rated current.

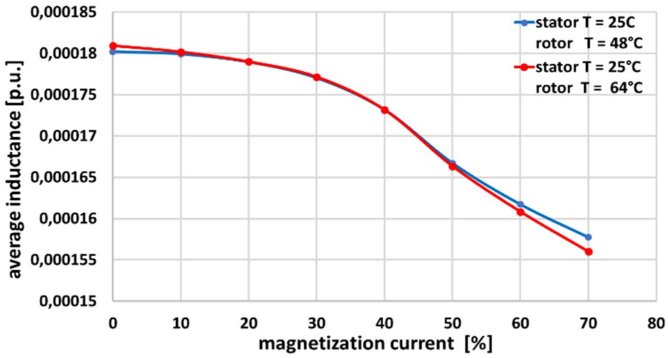

Fig. 10. Characteristic of average inductance over magnetizing current for different rotor temperatures and constant stator temperature of 28°C. Magnetizing current is expressed as percentage of rated current.

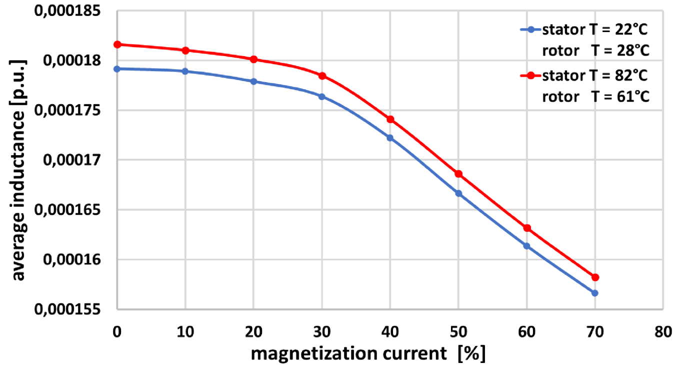

Fig. 11. Characteristic of average inductance over magnetizing current for different temperatures of the machine. Magnetizing current is expressed as percentage of rated current.

saturation. Within the investigated range of magnetization current, no point of intersection is visible.

V. CONCLUSION

Measurements, based on voltage pulse excitation and resulting current reaction measurement, conducted on a standard IM for railway applications indicate significant temperature dependences of magnetic properties. These dependences are consistent with investigations in different material probes found in several previous publications. The measurement procedure, initially developed for speed sensorless control, enables very accurate estimation of machines transient inductance. Specific measurements started with zero magnetization and different rotor and stator temperatures of the machine. Analyses show that initial inductance increases with temperature. For various stator temperatures and constant rotor temperature, this increase is 0.12‰/°C. With various rotor temperature and constant stator temperature, the increase amounts to 0.26‰/°C. The rising inductance is caused by the temperature dependence of the electrical steel sheet's permeability. This behavior is denoted Hopkinson effect in literature.

Further measurements were conducted with different levels of magnetization current and temperatures. Again, these measurements have shown that permeability increases with rising rotor and/or stator temperature at lower range of magnetization current. This dependence is weakened for higher levels of magnetization and finally undergoes a reversal when the electrical steel sheet is magnetically saturated. This suggests that flux density declines with temperature in case of saturated machine.

For rotor parameter identification and estimation of flux linkage commonly the assumption is made that inductance remains constant over temperature. The results achieved in this study can thus be used to improve accuracy of these techniques.

ACKNOWLEDGMENT

This research is supported Austrian Research Promotion Agency (FFG) under the Bridge-program, grant no. 858502. The authors want to thank Bombardier Transportation-COO Equipment organization, especially Mr. H. Mannsbarth (global head of BT_COO Equipment_Module Center Bogies & Drives). Special thanks for his generous support and technical feedbacks goes to Mr. M. Bazant (head of Plattform & Product Mgmt-DRIVES in BT_COO Equipment_Module Center Bogies & Drives). Furthermore the authors want to thank colleagues from Bombardier Transportation BT_COO Equipment(Dr. N. Weyrich, Mr. Chr. Wirth, Mr. U. Sorg, and Mr. A Bree), as well as Prof. Dr. H. Ertl (TU-Wien) for all their feedback and support. The authors further are very indebted to LEM group (especially Mr. A. Hürlimann/Chairman of Board of Directors, Dr. W. Teppan & Mr. J. Burk) for the cooperation and generous support.

REFERENCES

[1] W. Ying and G. Hongwei, "Induction-motor stator and rotor winding temperature estimation using signal injection method," IEEE Trans. Ind. Appl., pp. 1038–1044, (2006)

[2] C. Kyung-Rae and S. Jul-Ki, "Induction motor rotor temperature estimation based on a high-frequency model of a rotor bar," IEEE Trans. Ind. Appl., pp. 1267–1275, (2009)

[3] F. Briz, M. W. Degner, J. M. Guerrero and A. B. Diez, "Temperature estimation in inverter fed machines using high frequency carrier signal injection," IEEE Ind. Appl., pp. 799–808, (2008)

[4] W. Fahrner, M.A. Vogelsberger and T. Wolbank, "On-line Identification of Induction Machine Rotor (Parameters) in Speed Sensorless Operation based on Saliency Extraction," IEEE International Symposium on Power Electronics, Electrical Drives, Automation and Motion (SPEEDAM), (2018)

[5] W. Fahrner, M.A. Vogelsberger and T. Wolbank, "Sensorless On-line Rotor Parameter Detection of Induction Machines Based on Inverter Excitation," IEEE European Conference on Power Electronics and Applications (EPE), (2018)

[6] Morishita M., Takahashi N., Miyagi D. and Nakano M., "Examination of Magnetic Properties of Several Magnetic Materials at High Temperature," PRZEGLAD ELEKTROTECHNICZNY (Electrical Review), ISSN 0033-2097, R.87, (2011)

[7] N. Takahashi, M. Morishita, D. Miyagi and Nakano M., "Examination of Magnetic Properties of Magnetic Materials at High Temperature using a Ring Specimen," IEEE Trans. Magn., 46 pp. 548-551, (2010)

[8] Chikazumi S., and Graham C.D., "Physics of Ferromagnetism," Oxford University Press, (1997)

[9] Bozorth R. M., "Ferromagnetism," Van Nostrand D., (1951)

[10] D. Reigosa, F. Briz, C. Blanco and J.M. Guerrero, "Sensorless Control of Doubly-Fed Induction Generators Based on Stator High Frequency Signal Injection," IEEE Transactions on Industry Applications, pp. 3382-3391, (2014)

[11] R. A. N. Barroso and T. R. Fernandes Neto, "Sensorless torque control of an induction motor through quadrature voltage injection," IEEE Brazilian Power Electronics Conference (COBEP), pp. 1375- 1379, (2017)

[12] Q. Gao, G. M. Asher and M. Sumner, "Sensorless Position and Speed Control of Induction Motors Using High Frequency Injection and Without Offline Precommissioning", IEEE Transaction on Industrial Electronics, pp. 2474-2481, (2007)

[13] J. Ha and S.K. Sul, "Sensorless Field Orientation Control of an Induction Machine by High Frequency Signal Injection", IEEE IAS Annual Meeting, pp. 426-432, (1997)

[14] C. Spiteri, Staines, G.M. Asher and M. Sumner, "Sensorless Control of Induction Machines at Zero and Low Frequency using Zero Sequence Currents", IEEE Transactions on Industrial Electronics, pp. 195-206, (2005)

[15] H. Yang, Y. Zhang and P. D. Walker, "A Method to Start Rotating Induction Motor Based on Speed Sensorless Model-Predictive Control", IEEE Transaction on Energy Conversion, pp. 359-368 (2017)

[16] E. Zerdali and M. Barut, "The Comparisons of Optimized Extended Kalman Filters for Speed-Sensorless Control of Induction Motors," IEEE Transactions on Industrial Electronics, pp. 1-6, (2017)

[17] Y-D. Yoon and S-K. Sul, "Sensorless Control for Induction Machines Based on Square-Wave Voltage Injection", IEEE Transaction on Power Electronics, pp. 3637-3645, (2014)

[18] M. A. Vogelsberger, S. Grubic, Th. G. Habetler and Th. M. Wolbank, "Using PWM-Induced Transient Excitation and Advanced Signal Processing for Zero-Speed Sensorless Control of AC Machines," IEEE Transactions on Industrial Electronics pp. 365–374, (2010)

[19] B. Paya and P. Teixeira, "Electromagnetic characterization of magnetic steel alloys with respect to the temperature", 8th International Conference on Electromagnetic Processing of Materials, Cannes, France (2015)